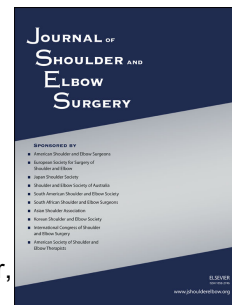


# Journal Pre-proof



Stemless Reverse Humeral Component Neck Shaft Angle has an Influence on Initial Fixation

David E. Cunningham, BEng, Gregory W. Spangenberg, BEng, G. Daniel G. Langohr, PhD, George S. Athwal, MD, FRCSC, James A. Johnson, PhD

PII: S1058-2746(23)00543-8

DOI: <https://doi.org/10.1016/j.jse.2023.06.035>

Reference: YMSE 6489

To appear in: *Journal of Shoulder and Elbow Surgery*

Received Date: 26 December 2022

Revised Date: 12 June 2023

Accepted Date: 24 June 2023

Please cite this article as: RRH: Neck Shaft Angle Affects Initial Fixation

This is a PDF file of an article that has undergone enhancements after acceptance, such as the addition of a cover page and metadata, and formatting for readability, but it is not yet the definitive version of record. This version will undergo additional copyediting, typesetting and review before it is published in its final form, but we are providing this version to give early visibility of the article. Please note that, during the production process, errors may be discovered which could affect the content, and all legal disclaimers that apply to the journal pertain.

© 2023 Published by Elsevier Inc. on behalf of Journal of Shoulder and Elbow Surgery Board of Trustees.

Running Title: Neck Shaft Angle Affects Initial Fixation

Title: **Stemless Reverse Humeral Component Neck Shaft Angle has an Influence on Initial Fixation**

David E. Cunningham, BEng<sup>a,b</sup>, Gregory W. Spangenberg, BEng<sup>a,b</sup>, G. Daniel G. Langohr, PhD<sup>a,b</sup>, George S. Athwal, MD, FRCSC<sup>b,c</sup>, James A. Johnson, PhD<sup>a,b,c,d,\*</sup>

<sup>a</sup>Department of Mechanical Engineering, The University of Western Ontario, London, ON, Canada

<sup>b</sup>The Roth|McFarlane Hand and Upper Limb Centre, St. Joseph's Hospital, London, ON, Canada

<sup>c</sup>Department of Surgery, The University of Western Ontario, London, ON, Canada

<sup>d</sup>Department of Biomedical Engineering, The University of Western Ontario, London, ON, Canada

Investigations performed at the Roth|McFarlane Hand and Upper Limb Center, London, ON, Canada

Institutional review board approval was not required for this basic science study.

#### **Disclaimers:**

Funding: No funding was disclosed by the authors.

Conflicts of interest: George S. Athwal is a consultant for DePuy-Synthes and Tornier (Wright Biomedical) and has received research support from Tornier (Wright Biomedical). The other authors, their immediate families, and any research foundation with which they are affiliated

have not received any financial payments or other benefits from any commercial entity related to the subject of this article.

Corresponding Author:

David E. Cunningham, BEng

dcunni9@uwo.ca

1151 Richmond St., London, ON N6A 3K7, Canada

p. 225-235-4860

## **Stemless Reverse Humeral Component Neck Shaft Angle has an Influence on Initial Fixation**

### 3 Abstract:

4 **Background:** Stemless anatomic humeral components are commonly used and are an accepted  
5 alternative to traditional stemmed implants in patients with good bone quality. Presently, little  
6 literature exists on the design and implantation parameters that influence primary time-zero  
7 fixation of stemless reverse humeral implants. Accordingly, this finite element analysis study  
8 assessed the surgical implantation variable of neck shaft angle, and its effect on the primary time-  
9 zero fixation of reversed stemless humeral implants.

**Methods:** Eight CT-derived humeral finite element models were used to examine a generic stemless humeral implant at varying neck shaft angles of 130°, 135°, 140°, 145°, and 150°. Four loading scenarios [30° shoulder abduction with neutral forearm rotation, 30° shoulder abduction with forearm supination, a head-height lifting motion, and a single-arm steering motion] were employed. Implantation inclinations were compared based on the maximum bone-implant interface distraction detected after loading.

16 **Results:** The implant-bone distraction was greatest in the 130° neck shaft angle implantation cases.  
17 All implant loading scenarios elicited significantly lower micromotion magnitudes when neck  
18 shaft angle was increased ( $P = 0.0001$ ). With every 5° increase in neck shaft angle, there was an  
19 average 17% reduction in bone-implant distraction.

20 **Conclusions:** The neck shaft angle of implantation for a stemless reverse humeral component is a  
21 modifiable parameter that appears to influence time zero implant stability. Lower, more varus,  
22 neck shaft angles increase bone-implant distractions with simulated activities of daily living. It is

23 therefore suggested that humeral head osteotomies at a higher neck shaft angle may be beneficial  
24 to maximize stemless humeral component stability.

25

26 **Level of evidence:** Basic Science Study; Computer Modeling

27 **Keywords:** stemless; neck shaft angle; arthroplasty; implant design; finite element; reverse  
28 shoulder arthroplasty; cuff tear arthropathy.

29

30

31 Reverse shoulder arthroplasty (RSA) implants have undergone a variety of design modifications  
32 since first introduced. Some modifications include press-fit stems, modularity, adjustments in neck  
33 shaft angle, and onlay/inlay design features. One design feature, focused on decreasing stress  
34 shielding and simplifying future revisions, has been the gradual shortening of the humeral stem<sup>30</sup>.

35

36 Although anatomical stemless shoulder arthroplasty implants are steadily becoming more popular,  
37 the use of stemless RSA implants is still limited, with very few published works reporting on the  
38 clinical and biomechanical performance of these novel implants<sup>1</sup>. Shorter humeral stem lengths  
39 have been shown to decrease stress shielding in periprosthetic bone by better mimicking natural  
40 force-transmission properties<sup>27</sup>. Stemless designs also benefit from the preservation of humeral  
41 bone stock, reduction of risk of periprosthetic fractures, and simplification of surgical technique<sup>26</sup>.  
42 However, these designs of humeral implant also pose several risks that emphasize the importance  
43 of primary fixation. Ultra-short implants or stemless humeral implants are more vulnerable to poor  
44 initial fixation, instability, or loosening than their stemmed counterparts, due to the reduced bone-  
45 implant contact area and lack of cortical bone contact<sup>1,26</sup>.

46

47 The primary method of achieving fixation in existing stemless RSA implants is via  
48 osseointegration (viz. bony ingrowth). In order for this bone-implant bonding to occur, the two  
49 surfaces are required to maintain limited relative motion (termed “micromotion”<sup>11,22</sup>) during the  
50 healing phase following surgery<sup>8</sup>. The tolerable threshold of shear micromotion is often quoted as  
51 150 µm<sup>3,6,10,20,26</sup>. However, the threshold of tolerable micromotion has also been reported as a  
52 range of between 30 µm<sup>15,20</sup> and 750 µm<sup>12,20</sup>. Additionally, it is rational to postulate that any lift-  
53 off or distraction micromotion may well impede bone contact and hence ingrowth.

54

55 One modifiable technical factor with stemless RSA humeral implants is the resection inclination  
56 angle (or neck shaft angle) of the humeral head. RSA systems with varied neck shaft angles (NSA)  
57 of between 127.5° and 155° are currently used. It has been found that decreasing NSA reduces the  
58 risk of scapular notching<sup>14</sup>, and that modifying NSA results in no significant differences in scapular  
59 spine strain<sup>16</sup>. In addition, it has previously been found that decreasing NSA significantly increases  
60 impingement-free range of motion<sup>35</sup>, providing incentive to decreasing NSA. However, there  
61 remains a lack of knowledge regarding the effect of NSA on primary implant fixation.

62

63 Computational methods have gained popularity in orthopedics due to their ability to estimate  
64 postoperative physical phenomena that are difficult to measure in-vivo<sup>4–9,13,28,30,31</sup>. Numerous  
65 computational studies evaluating implant designs are available<sup>4,27,28,30,34</sup>, however, little to no  
66 literature has evaluated the effect of neck shaft angle on primary reverse humeral implant fixation  
67 in-silico. The present investigation, therefore, determined the effect of stemless reverse humeral  
68 component insertion neck shaft angles on the primary time-zero stability of the implants. We

69 hypothesized that increasing neck shaft angle would result in better implant stability and decreased  
70 micromotion at the implant bone interface.

71

## 72 Methods

73 Computed tomography (CT) scans of eight shoulders from male cadaveric specimens (height: 177  
74  $\pm 4$  cm, weight:  $69 \pm 10$  kg) aged  $70 \pm 21$  years (mean  $\pm$  standard deviation) were collected using  
75 a clinical CT Scanner (slice thickness: 0.5 mm, pixel spacing:  $0.961 \times 0.961$  mm, exposure time:  
76 750 ms, kVp: 120) (GE 750HD Discovery Scanner; GE Healthcare, Chicago, IL, USA). A cortical  
77 bone surrogate (SB3 model 450; GAMMEX, Middleton, WI, USA), and distilled water were  
78 purposed as phantoms to calibrate the apparent density in  $\text{g/cm}^3$  from CT attenuation in Hounsfield  
79 units (HU)<sup>19</sup>. Three-dimensional models of the humerus (NSA:  $139^\circ \pm 6^\circ$ , retroversion:  $22^\circ \pm 13^\circ$ )  
80 and cortical shell were created in Mimics (Materialise, Leuven, Belgium) and exported as non-  
81 uniform rational basis spline (NURBS) models instead of stereolithography (STL) models since  
82 they can model complex surfaces on the bony anatomy with greater accuracy. A Boolean  
83 subtraction was performed to isolate the trabecular bone model from the humeral model in a  
84 subsequent step.

85

86 A generic stemless reverse implant design was developed using CadQuery, a 3D parametric design  
87 Python library<sup>25</sup> (Figure 1). This generic implant design was chosen as a general representation of  
88 a stemless boundary-crossing generic implant<sup>4,30</sup>; an amalgamation of the Reeves et al Quad-Peg  
89 boundary crossing generic implant<sup>30</sup>, as well as the Stryker Tornier, Zimmer Biomet, and Lima  
90 Corporate stemless designs currently available clinically. Anatomic generator implant examples

91 were utilized due to the lack of stemless reversed implants available clinically. A single size of  
92 generic implant (glenosphere diameter: 40 mm, collar diameter: 36 mm, penetrating volume:  
93 6.2 cm<sup>3</sup>) was found to be an acceptable fit for all humeral models used.

94

95 The generic implant model was positioned by a board-certified surgeon (GSA) in SolidWorks CAD  
96 software (Dassault Systèmes Corp., Waltham, MA, USA) at a 135° neck shaft angle. In order to  
97 maintain inclination consistency between specimens, the 135° implantation case was first  
98 positioned as a control, and a computational matrix transformation was utilized to vary inclination  
99 angle (at 130°, 135°, 140°, 145°, and 150° neck-shaft angles). A constant center of rotation,  
100 positioned at the most superior-lateral apex of the anatomical humeral neck in each specimen, was  
101 identified in the 135° control resection and utilized for NSA variation. Each humeral model was  
102 re-evaluated at every implantation condition. All implants were fully positioned in humeral  
103 trabecular bone, and no cortical contact was detected.

104

105 Finite element models were developed in Abaqus CAE 2021 software (Dassault Systèmes Corp.)  
106 using a previously validated approach<sup>27-29</sup>. All components were meshed with 1.2 mm quadratic  
107 tetrahedral elements, according to mesh convergence. Cortical bone was assigned a constant  
108 Young's modulus of 20 GPa<sup>18,23,28,30,32</sup>, and trabecular bone was assigned elastic moduli that varied  
109 in accordance to the Morgan et al density-elasticity relationship<sup>19,21,23,28,30,32</sup>. Mimics CT software  
110 was utilized to apply all inhomogeneous material properties to trabecular bone models ( $0.11 \pm 0.01$   
111 g/cm<sup>3</sup>, Pearson skew: 1.87). The cortical and trabecular bone models were both assigned a  
112 Poisson's ratio of 0.3<sup>6,28</sup>. The generic implant was assigned an elastic modulus of 110 GPa,  
113 representing titanium<sup>24,32</sup>, and a Poisson's ratio of 0.3<sup>6,28,30</sup>. Implant-bone contact was assumed as

114 frictional and modelled to represent the behaviour of a titanium plasma sprayed surface on bone  
115 ( $\mu = 0.6$ )<sup>26</sup>.

116

117 We employed four different loading scenarios [30° shoulder abduction with neutral forearm  
118 rotation, 30° shoulder abduction with forearm supination, a head-height lifting motion, and a  
119 single-arm steering motion] built from Orthoload patient-based measurements<sup>28</sup> to encompass a  
120 range of activities, particularly those known to produce eccentric loading, and therefore challenges  
121 to implant-bone fixation (Figure 2). These aforementioned activities were chosen as they represent  
122 a diverse array of loading states that a patient may experience immediately postoperatively while  
123 adhering to standard postoperative instruction. Loading data was extracted and corrected for the  
124 individual body weight of each subject<sup>7,28,30</sup>. The joint force line-of-action was directed through  
125 the center of rotation of the simulated reverse arthroplasty joint, and the humeral models were  
126 assigned encastre boundary conditions on a plane 50 mm distal to the neck shaft angle center of  
127 rotation (Figure 2).

128

## 129 **Analysis**

130 In order to quantify the initial fixation of each implantation case, the maximum normal bone-  
131 implant distraction (micromotion) was assessed. A one-way repeated measures analysis of  
132 variance (ANOVA), and a supplementary two-way repeated measures ANOVA with Bonferroni  
133 correction were conducted for the dependent variable of neck shaft angle for each loading scenario.  
134 All statistical analyses were computed using SciPy 1.9.1<sup>33</sup>, with the threshold of significance set  
135 as  $p < 0.05$ .

136 **Results**

137 Stemless humeral implants exhibit greater stability when implanted at higher neck-shaft angles.  
138 At higher neck shaft angles, a larger portion of the implant maintained contact with the cancellous  
139 epiphyseal and metaphyseal bone (Figure 3A) when compared to lower, more vertical, neck shaft  
140 angles (Figure 3B). For all loading cases, the maximum micromotion was detected on the  
141 periphery of the implant baseplate opposite to the direction of loading, while a greater portion of  
142 the implant maintained contact with bone at higher, more horizontal, neck shaft angles (Figure 4).  
143 The repeated measures ANOVA analysis revealed that the maximum micromotion developed at  
144 the implant-bone interface was significantly higher for the 130° neck shaft angle implantation  
145 conditions (30° shoulder abduction with neutral forearm rotation:  $p = 0.0192$ , 30° shoulder  
146 abduction with forearm supination:  $p < 0.0001$ , single handed steering motion:  $p = 0.0002$ , head-  
147 height lifting motion:  $p = 0.0038$ ) (Figure 5)(Table 1). During a supplementary two-way repeated  
148 measures ANOVA, Bonferroni correction with an adjusted alpha level of 0.025 (0.05/2) per test  
149 was utilized to further investigate the significance of neck-shaft angle. Results suggest that across  
150 all loading scenarios, neck-shaft angle significantly affected initial implant stability ( $p < 0.0001$ ).  
151

152 With every 5° increase in neck shaft angle, there was an average 14% decrease in the micromotion  
153 (30° shoulder abduction with neutral forearm rotation: 11.2%, 30° shoulder abduction with  
154 forearm supination: 13.5%, single handed steering motion: 18.5%, head-height lifting motion:  
155 14.0%) developed during loading.

156

157 **Discussion**

158 The principal objective of this work was to assess how humeral resection inclination (or neck shaft  
159 angle) may affect the primary stability of stemless reverse humeral implants. We specifically  
160 hypothesized that increasing neck shaft angle, thereby decreasing implant inclination, would elicit  
161 a more favorable level of implant stability than is experienced at lower neck shaft angles. Our  
162 results identified that variations in the neck shaft angle substantially influence time zero stemless  
163 implant fixation and stability.

164

165 From the results of this investigation, we postulate that increasing the neck shaft angle and the  
166 potential improvement for stemless implant fixation may in part be attributed to the line-of-action  
167 of the joint loading vector relative to the implant-bone interface. With a more horizontal (higher  
168 neck shaft angle) the joint loading vector passes closer to the center of the interface, reducing  
169 eccentric loading. Hence, the implant experiences a greater amount of compression into the  
170 proximal humeral bone and less distraction or lift-off. With a more vertical neck shaft angle, the  
171 implant does also experience compression, however, there is also a greater amount of eccentric  
172 loading. These eccentric loads, with a lower neck shaft angle, result in substantially greater amount  
173 of distraction of the implant anteriorly. Distraction, as a mechanism of failure, would clinically  
174 present as lift off of the implant anteriorly or flipping out of the implant.

175

176 We also postulate that bone quality may be influential, as altering the neck shaft angle affects the  
177 native bone stock present at the bone-implant interface. Reeves *et al*<sup>29</sup> have shown that the best  
178 quality bone in the proximal humerus is located peripherally in the metaphysis and in the humeral  
179 head. As such, we postulate that a higher neck shaft angle resection preserves a wedge of higher  
180 quality bone behind at the medial calcar region<sup>29</sup> (Figure 6). Therefore, a stemless humeral implant

181 placed at a higher neck shaft angle is typically inset into better quality bone in the medial calcar  
182 area than it would be at a lower neck shaft angle.

183

184 Alterations in neck shaft angle do have other important ramifications. Higher neck shaft angles  
185 result in greater humeral distalization, adduction impingement, possible notching, reduced  
186 abduction impingement and reduced internal/external rotation<sup>2,14</sup>. In contrast, lower neck shaft  
187 angles result in greater humeral offset, improved adduction motion and rotation, and a higher  
188 potential for abduction impingement<sup>2,17</sup>. All of the above factors should be considered when  
189 selecting a particular neck shaft angle.

190

191 There are limitations with the present work. A generic stemless implant design was assessed  
192 instead of implants currently available in the global market, which may lessen the clinical  
193 significance of these findings. The use of a generic implant ensured that full control over implant  
194 variables could be maintained and could therefore align with the initial hypothesis. This provided  
195 unbiased insight into how neck shaft angle may affect primary stability of stemless humeral  
196 implants. Future investigations should continue to assess additional implant designs in order to  
197 provide a more thorough evaluation on the load transfer effects of varying neck shaft angle.

198 Another possible limitation of this work is the small sample size utilized. Future investigations  
199 should use a larger cohort of patient CTs in order to better represent the global population.  
200 However, the use of 8 specimens is higher than typically employed for computational studies of  
201 this nature on implant-bone stress analyses. Additionally, this evaluation was focused on time-  
202 zero (directly after implantation) implant behaviors. This is noteworthy, as trabecular bone is  
203 mechanoresponsive, and the differences in loading postoperatively may result in changes to the

204 osseointegration responses in bone during the postoperative rehabilitation period. Specifically, in  
205 press-fit implants, experimental analyses focused on the effect of cyclical loading may provide  
206 valuable insight into the failure mechanisms of stemless humeral implants.

207

208 Strengths of this work include the repeated measures study design, with each specimen  
209 reconstructed repeatedly with varying neck shaft angles. This produced a more robust statistical  
210 power. The loads applied were also based on in-vivo telemetized data. While this data was  
211 collected for an anatomical total shoulder arthroplasty implant, in-vivo data for RSA does not yet  
212 exist. The same general loading scenarios adapted for RSA kinematics, should not be markedly  
213 different.

214

## 215 **Conclusion**

216 The neck shaft angle of implantation for a stemless reverse humeral component is a modifiable  
217 parameter that has a substantial effect on time zero implant stability. Lower, more varus, neck  
218 shaft angles increase bone-implant distractions with simulated activities of daily living. It is  
219 therefore suggested that in cases where primary reverse stemless implant stability is to be  
220 maximized for fixation, humeral head osteotomies at a higher neck shaft angle may be beneficial.

221

## 222 **Acknowledgments**

223 The authors acknowledge support provided by Natural Sciences and Engineering Research  
224 Council of Canada, the St. Joseph's Healthcare Roth McFarlane Hand and Upper Limb Center,  
225 and The University of Western Ontario, London, ON, Canada.

**References:**

1. Ajibade DA, Yin CX, Hamid HS, Wiater BP, Martusiewicz A, Wiater JM. Stemless reverse total shoulder arthroplasty: a systematic review. *J. Shoulder Elbow Surg.* 2022;31(5):1083–1095. Available from: <https://doi.org/10.1016/j.jse.2021.12.017>
2. Arenas-Miquelez A, Murphy RJ, Rosa A, Caironi D, Zumstein MA. Impact of humeral and glenoid component variations on range of motion in reverse geometry total shoulder arthroplasty: a standardized computer model study. *J. Shoulder Elbow Surg.* 2021;30(4):763–771. Available from: <https://doi.org/10.1016/j.jse.2020.07.026>
3. ASTM. ASTM F2028-17 Standard Test Methods for Dynamic Evaluation of Glenoid Loosening or Disassociation. 2018;1–15. doi:10.1520/F2028-17.Copyright
4. Bae TS, Ritzer EE, Cho W, Joo W. Effect of fin length and shape of stemless humeral components in a reverse shoulder implant system: a FEA study. *J. Mech. Sci. Technol.* 2021;35(1):417–422. doi:10.1007/s12206-020-1241-x
5. Bankoff ADP. Biomechanical Characteristics of the Bone In: Human Musculoskeletal Biomechanics. 2012. p. 61–85. Available from: <https://www.intechopen.com/books/advanced-biometric-technologies/liveness-detection-in-biometrics> doi:<https://doi.org/10.5772/19690>
6. Bonnevieille N, Geais L, Müller JH, Berhouet J. Effect of RSA glenoid baseplate central fixation on micromotion and bone stress. *JSES Int.* 2020;4(4):979–986. doi:10.1016/j.jseint.2020.07.004
7. Damm P, Dymke J. Orthoload Database Jul. Wolff Inst. 2021 [cited 2021 Jul 26]; Available from: <https://orthoload.com/database/>
8. Favre P, Henderson AD. Prediction of stemless humeral implant micromotion during upper limb activities. *Clin. Biomech.* 2016;36:46–51. doi:10.1016/j.clinbiomech.2016.05.003
9. Favre P, Perala S, Vogel P, Fucentese SF, Goff JR, Gerber C, et al. In vitro assessments of reverse glenoid stability using displacement gages are misleading - Recommendations for accurate measurements of interface micromotion. *Clin. Biomech.* 2011;26(9):917–922. doi:10.1016/j.clinbiomech.2011.05.002
10. Favre P, Seebek J, Thistleton PAE, Obrist M, Steffens JG, Hopkins AR, et al. In vitro initial stability of a stemless humeral implant. *Clin. Biomech.* 2016;32:113–117. doi:10.1016/j.clinbiomech.2015.12.004
11. Formaini NT, Everding NG, Levy JC, Santoni BG, Nayak AN, Wilson C. Glenoid baseplate fixation using hybrid configurations of locked and unlocked peripheral screws. *J. Orthop. Traumatol.* 2017;18(3):221–228. doi:10.1007/s10195-016-0438-3
12. Goodman S, Wang J-S, Doshi A, Aspenberg P. Difference in bone ingrowth after one versus two daily episodes of micromotion: Experiments with titanium chambers in rabbits. *J. Biomed. Mater. Res.* 1993;27(11):1419–1424.
13. Hopkins AR, Hansen UN, Bull AMJ, Emery R, Amis AA. Fixation of the reversed shoulder prosthesis. *J. Shoulder Elbow Surg.* 2008;17(6):974–980. doi:10.1016/j.jse.2008.04.012
14. Jeon BK, Panchal KA, Ji JH, Xin YZ, Park SR, Kim JH, et al. Combined effect of change

- in humeral neck-shaft angle and retroversion on shoulder range of motion in reverse total shoulder arthroplasty - A simulation study. *Clin. Biomech.* 2016;31:12–19. doi:10.1016/j.clinbiomech.2015.06.022
15. Kawahara H, Kawahara D, Hayakawa M, Tamai Y, Kuremoto T, Matsuda S. Osseointegration under immediate loading: Biomechanical stress-strain and bone formation-resorption. *Implant Dent.* 2003;12(1):61–68. doi:10.1097/01.ID.0000034394.75768.E3
16. Kerrigan AM, Reeves JM, Langohr GDG, Johnson JA, Athwal GS. The influence of reverse arthroplasty humeral component design features on scapular spine strain. *J. Shoulder Elbow Surg.* 2021;30(3):572–579. doi:10.1016/j.jse.2020.06.011
17. Kim DM, Aldeghaither M, Alabdullatif F, Shin MJ, Kholine E, Kim H, et al. Loosening and revision rates after total shoulder arthroplasty: A systematic review of cemented all-polyethylene glenoid and three modern designs of metal-backed glenoid. *BMC Musculoskelet. Disord.* 2020;21(1):1–16. doi:10.1186/s12891-020-3135-6
18. Knowles N. Improving Material Mapping in Glenohumeral Finite Element Models: A Multi-Level Evaluation. Electron. Thesis Diss. Repos. 2019; Available from: <https://ir.lib.uwo.ca/etd/6100>
19. Knowles NK, Reeves JM, Ferreira LM. Quantitative Computed Tomography (QCT) derived Bone Mineral Density (BMD) in finite element studies: a review of the literature. *J. Exp. Orthop.* 2016;3(1). doi:10.1186/s40634-016-0072-2
20. Kohli N, Stoddart JC, van Arkel RJ. The limit of tolerable micromotion for implant osseointegration: a systematic review. *Sci. Rep.* 2021;11(1):1–11. doi:10.1038/s41598-021-90142-5
21. Mahaffy MD. Examining Reverse Total Shoulder Arthroplasty Baseplate Fixation in Patients with E2-type Glenoid Erosion Keywords. 2018;
22. Martin EJ, Duquin TR, Ehrenberger MT. Reverse total shoulder glenoid baseplate stability with superior glenoid bone loss. *J. Shoulder Elbow Surg.* 2017;26(10):1748–1755. doi:10.1016/j.jse.2017.04.020
23. Morgan EF, Bayraktar HH, Keaveny TM. Trabecular bone modulus-density relationships depend on anatomic site. *J. Biomech.* 2003;36(7):897–904. doi:10.1016/S0021-9290(03)00071-X
24. Navarro M, Michiardi A, Castaño O, Planell JA, Interface JRS, Navarro M, et al. Biomaterials in orthopaedics Biomaterials in orthopaedics. *J. R. Soc. Interface.* 2008;5:1137–1158. doi:10.1098/rsif.2008.0151
25. Parametric Products. CadQuery 2022; Available from: <https://github.com/CadQuery/cadquery>
26. Quental C, Folgado J, Comenda M, Monteiro J, Sarmento M. Primary stability analysis of stemless shoulder implants. *Med. Eng. Phys.* 2020;81:22–29. doi:10.1016/j.medengphy.2020.04.009
27. Razfar N. Finite Element Modeling of the Proximal Humerus to Compare Stemless , Short and Standard Stem Humeral Components of Varying Material Stiffness for Shoulder Arthroplasty Univ. West. Ontario - Electron. Thesis Diss. Repos. 2014;2431. Available from: <https://ir.lib.uwo.ca/etd/2431>
28. Razfar N, Reeves JM, Langohr DG, Willing R, Athwal GS, Johnson JA. Comparison of proximal humeral bone stresses between stemless, short stem, and standard stem length: A finite element analysis. *J. Shoulder Elbow Surg.* 2016;25(7):1076–1083.

- doi:10.1016/j.jse.2015.11.011
- 29. Reeves JM. An In-Silico Assessment of Stemless Shoulder Arthroplasty: from An In-Silico Assessment of Stemless Shoulder Arthroplasty: from CT to Predicted Bone Response CT to Predicted Bone Response 2018;Available from: <https://ir.lib.uwo.ca/etdhttps://ir.lib.uwo.ca/etd/5398>
  - 30. Reeves JM, Langohr GDG, Athwal GS, Johnson JA. The effect of stemless humeral component fixation feature design on bone stress and strain response: a finite element analysis. *J. Shoulder Elbow Surg.* 2018;27(12):2232–2241. doi:10.1016/j.jse.2018.06.002
  - 31. Suárez DR, Nerkens W, Valstar ER, Rozing PM, van Keulen F. Interface micromotions increase with less-conforming cementless glenoid components. *J. Shoulder Elbow Surg.* 2012;21(4):474–482. doi:10.1016/j.jse.2011.03.008
  - 32. Synnott S. The Effect of Implant Girth and Implant Collar on the Degree of Bone to Implant Contact and Bone Stresses in the Proximal Humerus. 2018;
  - 33. Virtanen P, Gommers R, Oliphant TE, Haberland M, Reddy T, Cournapeau D, et al. SciPy 1.0: fundamental algorithms for scientific computing in Python. *Nat. Methods.* 2020;17(3):261–272. doi:10.1038/s41592-019-0686-2
  - 34. Wahab AHA, Saad APM, Syahrom A, Kadir MRA. In silico study of glenoid perforation during total shoulder arthroplasty: the effects on stress & micromotion. *Comput. Methods Biomed. Engin.* 2020;23(5):182–190. doi:10.1080/10255842.2019.1709828
  - 35. Werner BS, Chaoui J, Walch G. The influence of humeral neck shaft angle and glenoid lateralization on range of motion in reverse shoulder arthroplasty. *J. Shoulder Elbow Surg.* 2017;26(10):1726–1731. doi:10.1016/j.jse.2017.03.032

### Figures:

Figure 1: A posterior-lateral view of the left humerus implanted with a generic boundary-crossing implant, designed using variable-driven parametric design software. The implant was repetitively positioned into all 3D humeral models, developed from patient CT scans, at each neck shaft angle.

Figure 2: Four loading scenarios representing common activities of daily living that a patient might experience postoperatively ( $30^\circ$  shoulder abduction with neutral forearm rotation ( $30^\circ$  ABD – N),  $30^\circ$  shoulder abduction with forearm supination ( $30^\circ$  ABD – S), a head-height lifting motion (HHL), and a single-arm steering motion (SHS)). Each load was applied to a point consistent with the center of the glenosphere in the total reversed total shoulder arthroplasty reconstruction. Encastre boundary conditions are depicted at the distal humeral resection surface using striped boxes.

Figure 3: Posterior-Lateral view of the left humerus, implanted with a generic stemless implant at  $150^\circ$  (A) and  $130^\circ$  (B), with a heatmap of bone-implant distraction magnitude overlayed. A lateral

resection-view is also displayed in the bottom left corner of each subplot. For illustration purposes, the micromotion heatmap resulting from a single hand steering motion is shown.

Figure 4: Heatmaps of the micromotions developed at the bone-implant interface ( $N = 1$ ). All plots shown above are visualized medial-laterally at a view normal to the  $135^\circ$  neck shaft angle resection surface. Maximum micromotions were detected at the bone-implant interface at a position opposite to the direction of loading, indicated by the blue cross markings. Areas without coloured nodes did not move relative to bone throughout the analysis.

Figure 5: Maximum micromotion (mean  $\pm$  1 SD) levels for the four simulated activities at five neck shaft angles.

Figure 6: A stemless implant placed at a  $145^\circ$  neck shaft angle. The resultant resection at  $145^\circ$  leaves a wedge of higher quality medial calcar bone behind (blue arrow) for improved implant stability and fixation when compared with the  $135^\circ$  neck shaft angle resection.

### Tables:

Table 1: Interface micromotion parameters for varying implantation neck shaft angles. Each neck shaft angle ( $130^\circ$  -  $150^\circ$ ) was evaluated at loads representative of four activities of daily living.

**Table 1.** Interface micromotion parameters for varying implantation neck shaft angles. Each neck shaft angle (130° - 150°) was evaluated at loads representative of four activities of daily living.

	Micromotion ( $\mu\text{m}$ )									
	130°		135°		140°		145°		150°	
	Mean (SD)	Range	Mean (SD)	Range	Mean (SD)	Range	Mean (SD)	Range	Mean (SD)	Range
30° shoulder abduction with neutral forearm rotation	4.19 (2.77)	2.29 – 10.77	3.40 (1.99)	2.21 – 8.53	3.05 (1.43)	2.20 – 6.70	2.83 (1.07)	1.76 – 5.25	2.59 (0.80)	1.80 – 4.62
30° shoulder abduction with forearm supination	33.71 (8.01)	24.08 – 48.09	31.06 (8.36)	21.74 – 47.38	27.66 (7.86)	19.11 – 42.47	23.32 (7.15)	16.60 – 36.97	18.80 (6.50)	12.06 – 30.91
Single handed steering motion	26.66 (19.94)	6.74 – 70.31	19.79 (15.16)	7.05 – 56.55	16.23 (11.70)	7.42 – 45.75	13.81 (9.12)	7.51 – 36.94	11.68 (6.92)	7.72 – 29.64
Head-height lifting motion	17.39 (15.96)	4.28 – 54.28	14.33 (14.12)	3.53 – 49.08	12.11 (11.71)	3.95 – 41.56	11.17 (9.79)	4.56 – 35.02	9.47 (7.45)	5.24 – 28.69

